Randomized Benchmarking Using Nondestructive Readout in a Two-Dimensional Atom Array

B. Nikolov,* E. Diamond-Hitchcock, J. Bass, N. L. R. Spong, and J. D. Pritchard
Department of Physics and SUPA, University of Strathclyde, Glasgow G4 0NG, United Kingdom

(Received 25 January 2023; accepted 22 June 2023; published 19 July 2023)

Neutral atoms are a promising platform for scalable quantum computing, however, prior demonstration of high fidelity gates or low-loss readout methods have employed restricted numbers of qubits. Using randomized benchmarking of microwave-driven single-qubit gates, we demonstrate average gate errors of $7(2) \times 10^{-5}$ on a 225 site atom array using conventional, destructive readout. We further demonstrate a factor of 1.7 suppression of the primary measurement errors via low-loss, nondestructive, and state-selective readout on 49 sites while achieving gate errors of $2(9) \times 10^{-4}$.

DOI: 10.1103/PhysRevLett.131.030602

Neutral atoms have emerged as a competitive platform for scalable quantum computing [1–3], using arrays of optical tweezers or optical lattices to create deterministically loaded, defect-free qubit registers of atoms in up to three dimensions [4–8] in arrays with over 1000 sites [9]. Interactions between highly excited Rydberg states can be exploited to perform high-fidelity two- [10–16] or multi-qubit gate operations [14,17], with the ability to realize complex connectivities using movable tweezers [18]. As well as enabling recent demonstrations of quantum algorithms [18,19], this same platform can be exploited for quantum simulation [20–22] or analog quantum computation to address practical optimization problems [23,24].

An essential requirement for future fault-tolerant scaling is the ability to perform gate operations below the error threshold [25–27]. One approach to measuring the average gate errors is randomized benchmarking, originally proposed for trapped ions [28,29] and later adapted to a range of different hardware platforms [30–32]. This method averages performance over random strings of Clifford gates to extract both gate and readout errors. Randomized benchmarking has been used to characterize microwave-driven single-qubit gates in optical lattices [32–34] and tweezer arrays [35,36] of neutral atoms, but to date has only been demonstrated to exceed this threshold for a subset of 16 atoms [36].

A second requirement for future scaling is the ability to perform scalable and high-fidelity nondestructive readout (NDRO) to suppress measurement errors arising from the typical destructive readout scheme of ejecting atoms in qubit state $|1\rangle$ prior to imaging which cannot distinguish against atom loss during computation [37]. Significant progress has been demonstrated for NDRO of up to a few qubits using selective fluorescence in free-space [38–41], a high-finesse optical cavity [42–44], and atomic ensembles [45] permitting fast detection on 100 μs timescales with fidelities up to 0.999. However, quantum error correction necessitates repeated and parallel NDRO measurements of ancilla qubits in large arrays [46,47], presently only achieved using state-selective forces in a 3D lattice [48].

In this Letter we demonstrate randomized benchmarking combined with a non-destructive readout (NDRO) across a 2D array using a low-loss technique that allows simultaneous measurement of qubit state and presence to allow postselection against loss. First we showcase the capabilities of our experimental platform on a 225 trap site array by performing Clifford group randomized benchmarking with composite microwave (MW) pulses and a conventional, destructive readout process. Then, we implement NDRO on a 49 site array, limited by the available optical dipole trap (ODT) laser power required to create the higher trap depths needed during readout. Using this smaller array, we compare the randomized benchmarking performance obtained with conventional and nondestructive readout techniques. We demonstrate that we can efficiently transfer the atoms between the computational state $|1\rangle$, and the stretched state, where the nondestructive measurement takes place, using the NDRO beams. Finally, we discuss the limitations in the present NDRO performance and highlight experimental improvements to further reduce single atom losses. Combining this technique with long vacuum lifetime cryogenic systems [49] and atom sorting [4,5] could allow for the same atoms to be re-used for multiple experimental cycles leading to significantly faster repetition rates. This approach is also compatible with recent demonstration of mid-circuit measurement of

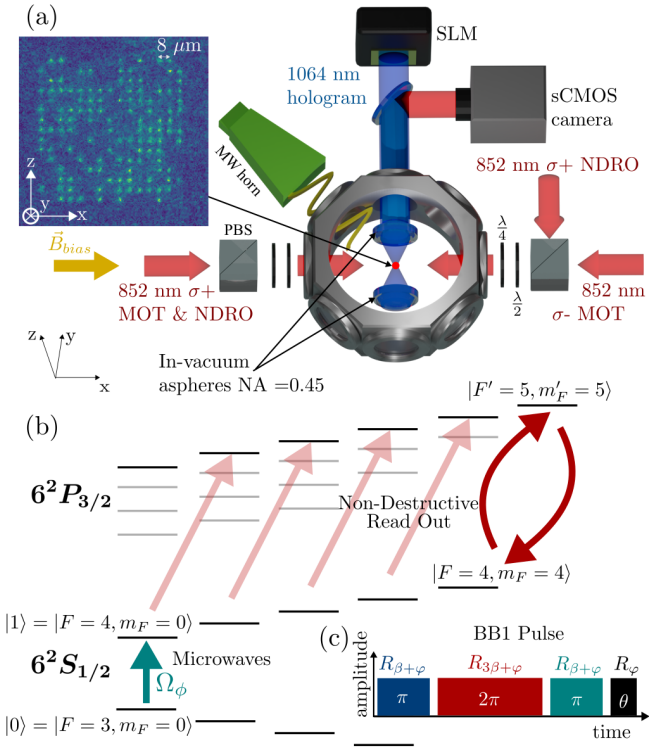

FIG. 1. (a) Experimental setup for randomized benchmarking and nondestructive readout (NDRO). Atoms are trapped in a 1064 nm tweezer array and imaged onto an sCMOS camera using in-vacuum high NA lenses. NDRO is applied using a pair of counterpropagating beams aligned along the quantization axis, with microwaves emitted from a horn antenna to realize global single-qubit rotations. (b) Energy level diagram showing relevant ^{133}Cs energy levels. Microwave gates are applied between hyperfine encoded clock qubits $|0\rangle$, $|1\rangle$. (c) Schematic of a robust BB1 composite pulse used to implement single qubit rotation during randomized benchmarking.

spectator qubits in a dual-species array [50] to achieve NDRO of ancilla qubits for quantum error correction.

The experiment setup is shown schematically in Fig. 1. A spatial-light-modulator (SLM) is used to generate a rectangular array of up to 15×15 ODTs with a 1.5 μm $1/e^2$ waist, separated by spacing of 8 μm. The ODT laser is an M Squared diode-pumped solid state laser system with a wavelength of 1064 nm, red-detuned from the ^{133}Cs D lines, which is linearly polarized along the quantization axis. The inset of Fig. 1(a) shows a typical fluorescence image obtained from stochastically loaded single atoms in the array, imaged using a Teledyne Photometrics PrimeBSI sCMOS camera with a 47% quantum efficiency at 852 nm and an ITO-coated, in-vacuum aspheric lens with NA = 0.45 [51] which is also used to focus the ODT arrays. The atoms are loaded into the traps stochastically due to light-assisted collisions [52], and in each experimental run we load each site with a probability of 0.55 meaning just over half the sites are occupied. Following atom loading at a trap depth of 3 mK, a cycle of light-assisted collisions is performed to obtain single site loading and cool the atoms to 22 μK. Atoms are then prepared in the $|1\rangle = |F = 4, m_F = 0\rangle$ state by optically pumping using π-polarized light driving $F = 4 \rightarrow F' = 4$ on the D_1 line with a fidelity of 0.971(9), using a bias field of 6 G to define quantization. We then adiabatically lower the ODT potential to 15 μK, resulting in a final atom temperature of 8 μK.

State-selective detection is initially performed with a single blow away beam resonant on the ^{133}Cs D_2 line. The beam selectively heats atoms in $|F = 4\rangle$ out of the trap and leaves atoms in $|F = 3\rangle$ unperturbed. Our destructive readout errors are 1.0(1)% for false positive detection in $|F = 3\rangle$ and 0.5(2)% for false negative detection in $|F = 4\rangle$. To suppress tensor light shifts and heating from the antitrapped excited states, during cooling, state preparation, and readout the light is modulated out of phase with the ODT light at a frequency of 1 MHz with a 50% duty cycle. Further details of the experimental setup and sequence timings are provided in the Supplemental Material [53].

Single qubit rotations are performed using a global microwave pulse at 9.2 GHz, derived by mixing a low phase-noise 8.95 GHz phase-locked dielectric oscillator with an agile direct digital synthesizer (DDS) operating at variable frequencies around 220 MHz. Unwanted frequency components are then removed using a bandpass filter. The filtered signal is amplified to 8 W and transmitted to the experiment using a free-space horn antenna. For the clock transition from $|1\rangle = |F = 4, m_F = 0\rangle \rightarrow |0\rangle = |F = 3, m_F = 0\rangle$ we obtain an averaged Rabi frequency of $\Omega/2\pi = 9.6$ kHz. Despite the 3 cm microwave wavelength, we observe a 3% spatial variation in microwave Rabi frequency across the 112 μm array due to internal reflections inside the chamber. To mitigate the impact of this variation we apply microwave rotations using the BB1 composite pulse technique introduced in [55], and shown schematically in Fig. 1(c). The BB1 protocol applies an arbitrary rotation θ around axis φ using the four-pulse sequence $R_{\varphi+\beta}(\pi)R_{3\varphi+\beta}(2\pi)R_{\varphi+\beta}(\pi)R_\varphi(\theta)$, where $\beta = \cos^{-1}(-\theta/4\pi)$. This sequence reduces the sensitivity to amplitude errors to sixth order, making it robust to changes in pulse amplitude of up to 10% [56]. Using the microwaves we also characterize the qubit coherence time at the reduced trap depth using Ramsey interferometry, yielding an array average of $T_2^* = 14.09(8)$ ms [53].

To characterize the single qubit gate fidelity, we apply a randomized benchmarking approach based on uniform sampling of the 24 gates comprising the Clifford group [29,35]. The specific gate set used in the experiment is obtained by building a complete set of Clifford gates from combinations of BB1 pulses implementing $R_{x,y}(\pm\pi/2)$ and $R_{x,y}(\pi)$, and is described in further detail in the Supplemental Material [53]. Rotations around z axis are implemented in software as virtual gates [57], where $R_z(\theta)$ corresponds to a shift in the phase of all subsequent $R_{x,y}$

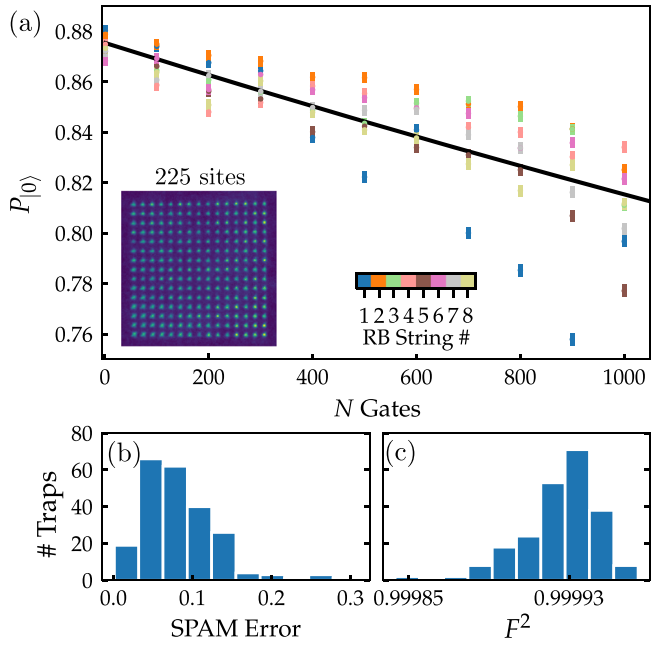

FIG. 2. Randomized benchmarking of 225 trap sites: (a) Array-averaged results from 8 different random gate strings with fit using Eq. (1). Histograms showing the distribution of (b) SPAM errors and (c) average gate fidelities, F^2, across the array. Error bars represent 1 standard deviation.

pulses equivalent to rotating the coordinate axes in the Bloch sphere. This results in an average area per gate of $\langle\theta\rangle_{C_1} = 2.95\pi$.

Using this experimental method, we generate 8 different random gate strings with a maximal length reaching up to $N = 1000$ gates. After applying the randomized sequence, a final correction pulse is applied to return the qubit to the $|0\rangle$ state, and the output populations are measured using 150 repeats for each data point. The total time allocated for microwave operations was fixed at 375 ms regardless of the number of gates applied in a given experimental run. The results of the randomized benchmarking on the 225-site array obtained using a destructive readout method are shown in Fig. 2(a) for each of the random gate strings. Error bars show 1 standard deviation. To extract the gate errors, a single fit function is applied to all data points using the equation

$$P_{|0\rangle} = \frac{1}{2} + \frac{1}{2}(1 - d_{\mathrm{SPAM}})(1 - d)^N, \tag{1}$$

where N is the number of random gates applied, d_{SPAM} is the state preparation and measurement error, and d is the average depolarization error per gate. For this conventional destructive readout approach $P_{|0\rangle}$ must be additionally scaled by the atom loss probability due to the finite trap lifetime of 9.7(8) s, which is independently measured to be 0.93(1) [53]. The averaged gate fidelity is then obtained from $F^2 = 1 - d/2$ [35]. Figures 2(b) and 2(c) show the distribution of SPAM error and fidelity across the array, with an array-averaged gate fidelity of $\langle F^2\rangle = 0.99\,993(2)$ (corresponding to an average error of 7×10^{-5}) and a maximum value of $F^2_{\mathrm{max}} = 0.99\,996(3)$ at a single array site.

These results represent the highest recorded averaged single qubit gate fidelities for any quantum computing platform with over 100 qubits. A lower average microwave single qubit gate error of $4.7 \pm 1.1 \times 10^{-5}$ has previously only been achieved in 4×4 arrays of ^{87}Rb atoms using magic polarization to suppress differential light shifts [36]. Our numbers are in good agreement with the theory from Ref. [35] which predicts $\langle F^2\rangle = 1 - \langle d\rangle/2 = 1 - [1 - \alpha(\langle t\rangle_{C_1}, T_2^*)]/2$, where $\alpha = 0.5 + 0.5[1 + 0.95(t/T_2^*)^2]^{-3/2}$ describes the loss of coherence due to dephasing [58] and $\langle t\rangle_{C_1} = \langle\theta\rangle_{C_1}/\Omega$ is the average Clifford gate duration. Using the values above we predict an error of 4×10^{-5}, with additional sources of error likely arising from magnetic field noise or residual phase-noise in the rf electronics.

A consequence of using BB1 pulses is the increased duration for longer gate sequences, which contributes to increased probability of loss due to background collisions and hence the high average SPAM error of 25% due to the inability to distinguish between a real qubit error with an atom left in $|1\rangle$ at the end of the sequence and an atom being lost during the computation.

To address this issue, we now introduce non-destructive state readout (NDRO) following the approach of [39,40]. Instead of applying a resonant blow-away pulse to remove atoms in $F = 4$, we perform a state-selective pulse using σ^+ polarized light on the D_2 $F = 4 \rightarrow F' = 5$ transition, which optically pumps atoms in $|1\rangle$ into the $|4, 4\rangle$ stretched-state to enable bright-state imaging on the cycling transition, while atoms in $|0\rangle$ are unaffected and remain dark. A subsequent imaging step is then performed using standard cooling and repump beams to verify the presence or absence of an atom in either hyperfine state to enable postselection for loss.

In the experiment, NDRO is implemented using a pair of counter-propagating beams oriented along the quantization axis as shown in Fig. 1(a). The beams are operated with a combined intensity equal to the saturation intensity $I_0 = 1.6$ mW/cm^2 and an average detuning of $\Delta/2\pi = -0.75\Gamma$ from the $|F = 4, m_F = 4\rangle \rightarrow |F' = 5, m'_F = 5\rangle$ transition. Where $\Gamma/2\pi = 5.2$ MHz is the excited state linewidth. The beams are operated with a relative frequency difference of 600 kHz to suppress standing-wave interference. As above, light is modulated out of phase with the ODT to suppress ac shifts and heating. The ODT is also polarized along the quantization axis to avoid fictitious magnetic fields [39].

Efficient NDRO requires maximizing the number of photons scattered to provide the maximal separation of bright and dark count rates for high-fidelity state detection, while minimizing losses due to heating on the cycling transition or leakage into $F = 3$ due to off-resonant scattering from imperfect polarization. We perform initial

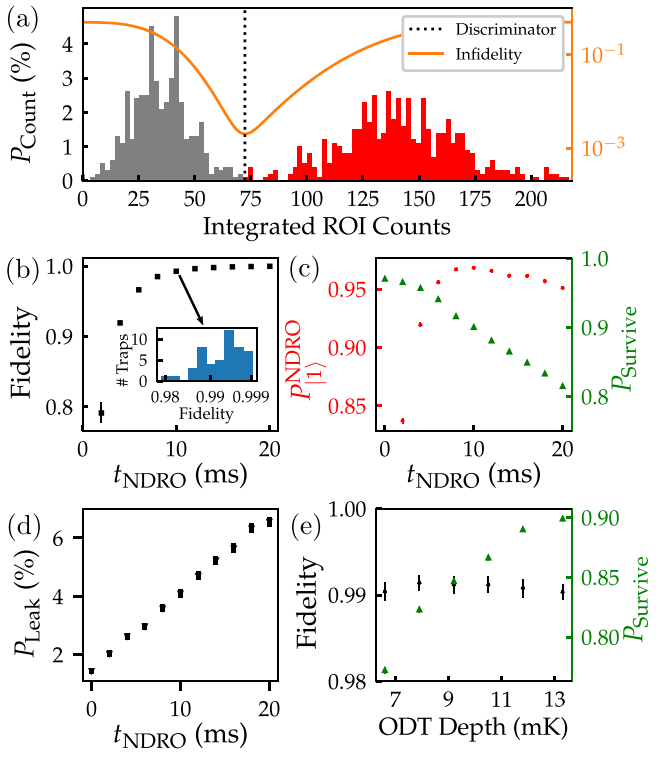

FIG. 3. NDRO characterization on 7×7 array at 13.3 mK trap depth. (a) Example NDRO histogram of integrated ROI counts for a single trap at $t_{\mathrm{NDRO}} = 10$ ms with dashed line showing threshold that maximises detection fidelity. (b) NDRO detection fidelity vs duration, with inset showing distribution across all traps at $t_{\mathrm{NDRO}} = 10$ ms. (c) NDRO detection ($P^{\mathrm{NDRO}}_{|1\rangle}$) and survival probabilities as a function of t_{NDRO}. (d) Leakage probability into $|F = 3\rangle$ during NDRO. From (b)–(d) we operate at $t_{\mathrm{NDRO}} =$ 10 ms to balance detection fidelity against errors from loss and leakage. (e) Survival and fidelity vs trap depth showing improved survival with trap depth while fidelity remains approximately constant.

optimization of NDRO parameters using a 7×7 array, adiabatically ramping the trap to a depth of 13.3 mK for the NDRO stage (limited by the available ODT power) to suppress losses. Figure 3(a) shows an example NDRO histogram obtained for 10 ms imaging duration, with red (gray) denoting counts from atoms initially prepared in the $|1\rangle(|0\rangle)$ state. From these histograms we determine the threshold value that minimizes false negative or positive errors, from which we can extract the detection fidelity. In Figs. 3(b)–3(d) we present experimental data for NDRO performance as a function of readout time t_{NDRO}. Figure 3(b) shows readout fidelity, (c) shows the probability of the atom surviving the readout process P_{Survival}, as well as the loss-corrected detection probability, $P^{\mathrm{NDRO}}_{|1\rangle}$, defined as the probability of being detected in $|1\rangle$ given the atom survived. Another important parameter is the impact of leakage into $F = 3$ during the readout process. To measure the leakage rate, we perform the NDRO sequence followed by resonant blow away to remove any atoms remaining in $F = 4$ prior to the final image, with results shown in Fig. 3(d). From these data we choose to operate at $t_{\mathrm{NDRO}} = 10$ ms, offering a compromise between the requirements with a 0.900(2) NDRO survival probability with a state detection fidelity of 0.9926(6). We obtain an NDRO detection probability $P^{\mathrm{NDRO}}_{|1\rangle} = 0.968(1)$, comparable to the measured state preparation fidelity for initializing atoms in the $|1\rangle$ state, and with a probability of leaking into $F = 3$ during readout of 4.1(1)%. The current state of the art performance for NDRO detection was reported in [41] with $99.91 \pm 0.02\%$ detection fidelity and 0.9(2)% detection driven loss for a single Cs atom using an adaptive detection scheme using a single photon counting module.

Finally, we investigate the effect of trap depth on atom retention after NDRO, which improves with increasing trap depth without compromizing discriminator fidelity as shown in Fig. 3(e). The final data point corresponds to 13.3 mK trap depth which is the maximum we can achieve for this array size with our current experimental setup, with further improvements expected with more laser power.

We now apply the randomized benchmarking using the same gate sequences as above on the smaller 7×7 array with NDRO detection, performing analysis now using the loss-corrected conditional probability $P^{\mathrm{NDRO}}_{|1\rangle}$ with results shown in Fig. 4. Using this readout scheme we achieve an array averaged fidelity of $\langle F^2 \rangle = 0.99978(9)$, in excellent

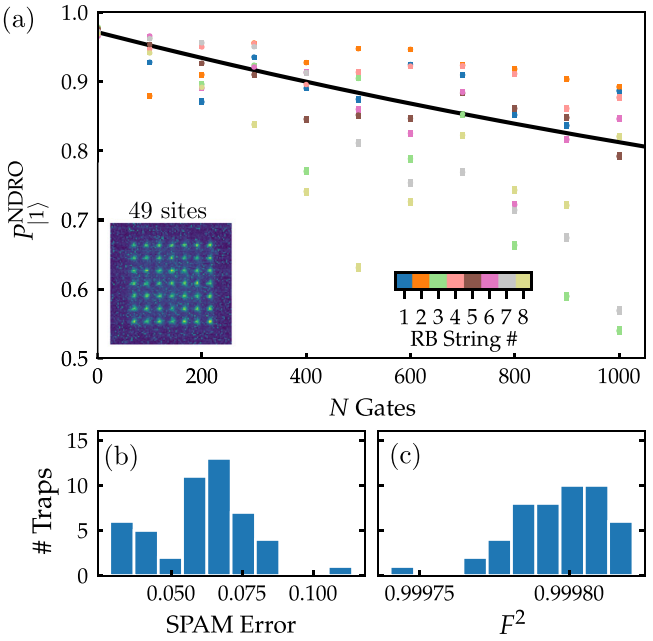

FIG. 4. (a) Randomized benchmarking results for 49 site array readout using NDRO from $|1\rangle$ state, postselected for survival. The same random gate strings were used as for the 225 site array. Distributions of (b) average gate fidelities and (c) SPAM errors obtained with a fit using Eq. (1).

agreement with the performance obtained in a repeated control measurement using the conventional readout sequence above with $\langle F^2 \rangle = 0.99\,978(1)$ [53]. The reduction in performance compared to the larger array is attributable to the finite extinction ratio of the ODT acousto-optic modulator meaning the microwave operations are performed at an increased trap depth, increasing the differential AC Stark shifts due to the ODT light from 39 to 211 Hz which results in a reduction of the coherence time for the smaller array $T_2^* = 12$ ms. The main improvement from the NDRO method comes from a factor of 1.7 reduction in SPAM error compared to the conventional readout with 225 sites. The SPAM error now amounts to $< 5\%$ as shown in Fig. 4(c). This is due to the removal of false positives corresponding to counting lost atoms as $|1\rangle$ during the readout process, with the dominant error now the finite state preparation fidelity.

In conclusion, we have demonstrated high fidelity single qubit gate operations with an average error of 7×10^{-5} by performing randomized benchmarking of global microwave pulses on an array with 225 sites using conventional, destructive detection. We have further demonstrated the ability to perform low-loss, nondestructive readout on an array of up to 49 qubits, and used the NDRO method to suppress SPAM errors due to the inability to discriminate against single atom loss. Already these operations are suitable for future fault-tolerant performance, but further improvements are possible using higher microwave powers to reduce the total gate time and considering additional composite or shaped pulse sequences to suppress frequency errors [56]. While previous experiments have achieved faster readout and lower loss for small numbers of qubits $\lesssim 5$ [39–41], we have demonstrated this NDRO technique can be scaled to larger 2D arrays.

NDRO performance is currently limited by the finite detection efficiency which limits the number of photon counts detected, and the limited trap depth during NDRO. In future, higher fidelity and reduced loss can be obtained by using an electron-multiplied CCD camera offering higher gain and quantum efficiencies $> 90\%$, or using a retroreflector to recover photons scattered away from the camera [40], to speed up readout and suppress heating. Similarly, changing to a magic wavelength trap at 935 nm to enable trapping of both ground and excited states [36] both eliminates the requirement for modulating the traps while increasing the effective trap depth from operating closer to resonance, corresponding to approximately 5 times more traps for the same total power.

These results extending high fidelity operations and NDRO readout to larger arrays are essential for realizing high-repetition rate digital computation by enabling atoms to be re-used after measurements, while also allowing for postselection against loss. These techniques can be combined with atom sorting to allow reloading of atoms lost during operations [4,5], and can be adapted for applications in quantum error correction for parallel readout of ancilla qubits [46,47] as required for fault-tolerant scaling.

The data presented in this work are available at [59].

The authors thank Andrew Daley and Arthur La Rooij for useful discussions. This work is supported by the EPSRC Prosperity Partnership *SQuAre* (Grant No. EP/T005386/1) with funding from M Squared Lasers Ltd.

*boyko.nikolov@strath.ac.uk

[1] M. Saffman, T. G. Walker, and K. Mølmer, Rev. Mod. Phys. **82**, 2313 (2010).
[2] C. S. Adams, J. D. Pritchard, and J. P. Shaffer, J. Phys. B **53**, 012002 (2019).
[3] M. Morgado and S. Whitlock, AVS Quantum Sci. **3**, 023501 (2021).
[4] M. Endres, H. Bernien, A. Keesling, H. Levine, E. R. Anschuetz, A. Krajenbrink, C. Senko, V. Vuletić, M. Greiner, and M. D. Lukin, Science **354**, 1024 (2016).
[5] D. Barredo, S. de Léséleuc, V. Lienhard, T. Lahaye, and A. Browaeys, Science **354**, 1021 (2016).
[6] D. Barredo, V. Lienhard, S. de Léséleuc, T. Lahaye, and A. Browaeys, Nature (London) **561**, 79 (2018).
[7] A. Kumar, T.-Y. Wu, F. Giraldo, and D. S. Weiss, Nature (London) **561**, 83 (2018).
[8] M. Schlosser, S. Tichelmann, D. Schäffner, D. O. de Mello, M. Hambach, J. Schütz, and G. Birkl, Phys. Rev. Lett. **130**, 180601 (2023).
[9] P. Huft, Y. Song, T. M. Graham, K. Jooya, S. Deshpande, C. Fang, M. Kats, and M. Saffman, Phys. Rev. A **105**, 063111 (2022).
[10] L. Isenhower, E. Urban, X. L. Zhang, A. T. Gill, T. Henage, T. A. Johnson, T. G. Walker, and M. Saffman, Phys. Rev. Lett. **104**, 010503 (2010).
[11] K. M. Maller, M. T. Lichtman, T. Xia, Y. Sun, M. J. Piotrowicz, A. W. Carr, L. Isenhower, and M. Saffman, Phys. Rev. A **92**, 022336 (2015).
[12] Y. Zeng, P. Xu, X. He, Y. Liu, M. Liu, J. Wang, D. J. Papoular, G. V. Shlyapnikov, and M. Zhan, Phys. Rev. Lett. **119**, 160502 (2017).
[13] T. M. Graham, M. Kwon, B. Grinkemeyer, Z. Marra, X. Jiang, M. T. Lichtman, Y. Sun, M. Ebert, and M. Saffman, Phys. Rev. Lett. **123**, 230501 (2019).
[14] H. Levine, A. Keesling, G. Semeghini, A. Omran, T. T. Wang, S. Ebadi, H. Bernien, M. Greiner, V. Vuletić, H. Pichler, and M. D. Lukin, Phys. Rev. Lett. **123**, 170503 (2019).
[15] Z. Fu, P. Xu, Y. Sun, Y. Y. Liu, X. D. He, X. Li, M. Liu, R. B. Li, J. Wang, L. Liu, and M. S. Zhan, Phys. Rev. A **105**, 042430 (2022).
[16] K. McDonnell, L. F. Keary, and J. D. Pritchard, Phys. Rev. Lett. **129**, 200501 (2022).
[17] G. Pelegrí, A. J. Daley, and J. D. Pritchard, Quantum Sci. Technol. **7**, 045020 (2022).
[18] D. Bluvstein, H. Levine, G. Semeghini, T. T. Wang, S. Ebadi, M. Kalinowski, A. Keesling, N. Maskara, H. Pichler, M. Greiner, V. Vuletić, and M. D. Lukin, Nature (London) **604**, 451 (2022).

[19] T. M. Graham *et al.*, Nature (London) **604**, 457 (2022).
[20] S. Ebadi, T. T. Wang, H. Levine, A. Keesling, G. Semeghini, A. Omran, D. Bluvstein, R. Samajdar, H. Pichler, W. W. Ho, S. Choi, S. Sachdev, M. Greiner, V. Vuletić, and M. D. Lukin, Nature (London) **595**, 227 (2021).
[21] P. Scholl, M. Schuler, H. J. Williams, A. A. Eberharter, D. Barredo, K.-N. Schymik, V. Lienhard, L.-P. Henry, T. C. Lang, T. Lahaye, A. M. Läuchli, and A. Browaeys, Nature (London) **595**, 233 (2021).
[22] G. Semeghini, H. Levine, A. Keesling, S. Ebadi, T. T. Wang, D. Bluvstein, R. Verresen, H. Pichler, M. Kalinowski, R. Samajdar, A. Omran, S. Sachdev, A. Vishwanath, M. Greiner, V. Vuletic, and M. D. Lukin, Science **374**, 1242 (2021).
[23] S. Ebadi *et al.*, Science **376**, 1209 (2022).
[24] M.-T. Nguyen, J.-G. Liu, J. Wurtz, M. D. Lukin, S.-T. Wang, and H. Pichler, PRX Quantum **4**, 010316 (2023).
[25] E. Knill, Nature (London) **434**, 39 (2005).
[26] A. M. Steane, Phys. Rev. Lett. **77**, 793 (1996).
[27] S. J. Devitt, W. J. Munro, and K. Nemoto, Rep. Prog. Phys. **76**, 076001 (2013).
[28] J. Emerson, R. Alicki, and K. Zyczkowski, J. Opt. B **7**, S347 (2005).
[29] C. Dankert, R. Cleve, J. Emerson, and E. Livine, Phys. Rev. A **80**, 012304 (2009).
[30] E. Knill, D. Leibfried, R. Reichle, J. Britton, R. B. Blakestad, J. D. Jost, C. Langer, R. Ozeri, S. Seidelin, and D. J. Wineland, Phys. Rev. A **77**, 012307 (2008).
[31] J. M. Chow, J. M. Gambetta, L. Tornberg, J. Koch, L. S. Bishop, A. A. Houck, B. R. Johnson, L. Frunzio, S. M. Girvin, and R. J. Schoelkopf, Phys. Rev. Lett. **102**, 090502 (2009).
[32] S. Olmschenk, R. Chicireanu, K. D. Nelson, and J. V. Porto, New J. Phys. **12**, 113007 (2010).
[33] J. H. Lee, E. Montano, I. H. Deutsch, and P. S. Jessen, Nat. Commun. **4**, 2027 (2013).
[34] Y. Wang, A. Kumar, T.-Y. Wu, and D. S. Weiss, Science **352**, 1562 (2016).
[35] T. Xia, M. Lichtman, K. Maller, A. W. Carr, M. J. Piotrowicz, L. Isenhower, and M. Saffman, Phys. Rev. Lett. **114**, 100503 (2015).
[36] C. Sheng, X. He, P. Xu, R. Guo, K. Wang, Z. Xiong, M. Liu, J. Wang, and M. Zhan, Phys. Rev. Lett. **121**, 240501 (2018).
[37] M. Saffman, J. Phys. B **49**, 202001 (2016).
[38] A. Fuhrmanek, R. Bourgain, Y. R. P. Sortais, and A. Browaeys, Phys. Rev. Lett. **106**, 133003 (2011).
[39] M. Kwon, M. F. Ebert, T. G. Walker, and M. Saffman, Phys. Rev. Lett. **119**, 180504 (2017).
[40] M. Martinez-Dorantes, W. Alt, J. Gallego, S. Ghosh, L. Ratschbacher, Y. Völzke, and D. Meschede, Phys. Rev. Lett. **119**, 180503 (2017).
[41] B. L. M. N. H. Chow and Y.-Y. Jau, arXiv:2206.00144.
[42] J. Bochmann, M. Mücke, C. Guhl, S. Ritter, G. Rempe, and D. L. Moehring, Phys. Rev. Lett. **104**, 203601 (2010).
[43] R. Gehr, J. Volz, G. Dubois, T. Steinmetz, Y. Colombe, B. L. Lev, R. Long, J. Estève, and J. Reichel, Phys. Rev. Lett. **104**, 203602 (2010).
[44] E. Deist, Y.-H. Lu, J. Ho, M. K. Pasha, J. Zeiher, Z. Yan, and D. M. Stamper-Kurn, Phys. Rev. Lett. **129**, 203602 (2022).
[45] W. Xu, A. V. Venkatramani, S. H. Cantú, T. Šumarac, V. Klüsener, M. D. Lukin, and V. Vuletić, Phys. Rev. Lett. **127**, 050501 (2021).
[46] J. M. Auger, S. Bergamini, and D. E. Browne, Phys. Rev. A **96**, 052320 (2017).
[47] I. Cong, H. Levine, A. Keesling, D. Bluvstein, S.-T. Wang, and M. D. Lukin, Phys. Rev. X **12**, 021049 (2022).
[48] T.-Y. Wu, A. Kumar, F. Giraldo, and D. S. Weiss, Nat. Phys. **15**, 538 (2019).
[49] K.-N. Schymik, S. Pancaldi, F. Nogrette, D. Barredo, J. Paris, A. Browaeys, and T. Lahaye, Phys. Rev. Appl. **16**, 034013 (2021).
[50] K. Singh, C. E. Bradley, S. Anand, V. Ramesh, R. White, and H. Bernien, Science **380** 1265 (2023).
[51] Y. R. P. Sortais, H. Marion, C. Tuchendler, A. M. Lance, M. Lamare, P. Fournet, C. Armellin, R. Mercier, G. Messin, A. Browaeys, and P. Grangier, Phys. Rev. A **75**, 013406 (2007).
[52] N. Schlosser, G. Reymond, and P. Grangier, Phys. Rev. Lett. **89**, 023005 (2002).
[53] See Supplemental Material at http://link.aps.org/supplemental/10.1103/PhysRevLett.131.030602, which includes Ref. [54] for single atom temperature measurement.
[54] C. Tuchendler, A. M. Lance, A. Browaeys, Y. R. P. Sortais, and P. Grangier, Phys. Rev. A **78**, 033425 (2008).
[55] S. Wimperis, J. Magn. Reson., Ser. A **109**, 221 (1994).
[56] G. Wolfowicz and J. J. Morton, Pulse techniques for quantum information processing, in *eMagRes* (John Wiley & Sons, Ltd, New York, 2016), p. 1515.
[57] D. C. McKay, C. J. Wood, S. Sheldon, J. M. Chow, and J. M. Gambetta, Phys. Rev. A **96**, 022330 (2017).
[58] S. Kuhr, W. Alt, D. Schrader, I. Dotsenko, Y. Miroshnychenko, A. Rauschenbeutel, and D. Meschede, Phys. Rev. A **72**, 023406 (2005).
[59] Boyko Nikolov *et al.*, Data for: "Randomized Benchmarking using Non-Destructive Readout in a 2D Atom Array" (2023), 10.15129/6dbdbc49-4053-43c6-ab08-9521e3618568.